Nano Research

ISSN 1998-0124 CN 11-5974/O4
https://doi.org/10.1007/s12274-023-5762-3

Research Article

Size effect enabling additive-free MXene ink with ultrahigh conductivity for screen printing of wireless electronics

Shuaishuai Chen[1,§], Huaqiang Fu[1,§], Yunfa Si[1], Xueyu Liu[2], Zhe Wang[1], Yixue Duan[1], Zixin Zhang[1], Hao Feng[1], Xin Zhao[2,3] (✉), and Daping He[1,2] (✉)

[1] *State Key Laboratory of Advanced Technology for Materials Synthesis and Processing, Wuhan University of Technology, Wuhan 430070, China*
[2] *Hubei Engineering Research Center of RF-Microwave Technology and Application, Wuhan University of Technology, Wuhan 430070, China*
[3] *School of Science, Wuhan University of Technology, Wuhan 430070, China*
[§] *Shuaishuai Chen and Huaqiang Fu contributed equally to this work.*

Received: 12 February 2023 / **Revised:** 28 March 2023 / **Accepted:** 5 April 2023

ABSTRACT

Facile preparation of additive-free inks with both high viscosity and high conductivity is critical for scalable screen printing of wireless electronics, yet very challenging. MXene materials exhibit excellent conductivity and hydrophilicity, showing great potential in the field of additive-free inks for screen printing. Here, we demonstrate the synthesis of additive-free two-dimensional (2D) titanium carbide MXene inks, and realize screen-printed MXene wireless electronics for the first time. The viscosity of MXene ink is solely regulated by tuning the size of MXene nanosheet without any additives, hence rendering the printed MXene film extremely high conductivity of 1.67×10^5 S/m and fine printing resolution down to 0.05 mm on various flexible substrates. Moreover, radio frequency identification (RFID) tags fabricated using the additive-free MXene ink via screen printing exhibit stable antenna reading performance and superb flexibility. This article, thus offers a new route for the efficient, low-cost and pollution-free manufacture of printable electronics based on additive-free MXene inks.

KEYWORDS

size effect, additive-free, MXene ink, screen printing, wireless electronics, radio frequency identification (RFID)

1 Introduction

The flourishing of various communication terminals and Internet of Things (IoTs) has greatly stimulated the demand for wireless electronics [1–3]. However, the scalable manufacturing of wireless electronics with high efficiency, low cost and environmental benignancy remains challenging [4–6]. Extensive efforts have been devoted to incorporate novel patterning techniques such as spray-masking and laser-scribing into conventional manufacturing of wireless electronics, however, still facing the problems of sophisticated procedures and harmful chemicals involved in metal etching [7–9].

Screen printing, on the other hand, offers a promising strategy for efficient, versatile and environmental-friendly manufacture of wireless electronics [10, 11]. To ensure the printing resolution and radiation performance of the printed antennas, the development of printing inks synchronizing high viscosity and high electrical conductivity is of crucial importance [12, 13]. Substantial progress has been made in screen-printing electronics based on silver/copper nanoparticle inks, conductive polymers inks and carbon-based inks (graphene, carbon nanotubes and carbon black) [14–19]. Nonetheless, only limited achievements have been reported in screen-printed wireless electronics due to insufficient conductivity of the existing inks ($< 10^5$ S/m) in which additives (such as surfactants or binders) are typically utilized to improve uniformity and viscosity [20]. The removal of additives and extra annealing steps also complicate the manufacturing process [21]. Therefore, additive-free inks with both high viscosity and high conductivity are of great significance for scalable, low-cost, pollution-free, yet efficient screen printing of wireless electronics.

MXenes are a family of two-dimensional (2D) materials with ultrahigh electrical conductivity and superior hydrophilicity [22, 23]. Hence, the MXene materials serve as a powerful candidate as additive-free inks for screen-printing wireless electronics. However, to date, most reports on MXene inks for screen printing involve the usage of additives to increase the viscosity, which inevitably decreases the conductivity [24–28]. The only reported additive-free MXene ink suffers from sediments of unetched precursors and multilayered MXene, resulting in relatively low conductivity (6×10^4 S/m), which cannot afford the application of wireless electronics [29]. The main challenge of realizing MXene-based screen-printed wireless electronics thus lies in achieving high viscosity and high conductivity simultaneously [30, 31].

Herein, we developed an additive-free MXene ink and realized screen-printed wireless electronics using MXene ink for the first time. By synthesizing MXene inks composing of different sizes of nanosheets, we discovered that the large-size MXene nanosheets yield the MXene inks with higher viscosity and conductivity compared to the small-size MXene nanosheets in the absence of additives. High-resolution screen printing (0.05 mm) has been demonstrated on various substrates and an ultrahigh conductivity of 1.67×10^5 S/m has been achieved for the printed films, which is

Address correspondence to Xin Zhao, xzhao@whut.edu.cn; Daping He, hedaping@whut.edu.cn

the highest reported value of MXene-based 2D materials. Further, we fabricated radio frequency identification (RFID) tag antennas using the additive-free MXene inks via screen printing with excellent antenna reading distance and flexibility. Our findings of the size-dependent viscosity and conductivity of MXene inks offer a direction of preparing highly conductive and additive-free MXene inks suitable for screen printing of electronic devices such as wireless electronics, current collectors and energy storage devices.

2 Results and discussion

2.1 Characterization of MXene ink

Scanning electron microscopy (SEM) images shown in Figs. 1(a)–1(c) revealed different size distributions for the three types of MXene inks. The L-MXene ink exhibited the largest flake size of 10.7 μm among the three samples (Fig. 1(a) and Fig. S1(a) in the Electronics Supplementary Materials (ESM)). The other two samples (denoted as S2-MXene ink and S1-MXene ink) exhibited average flake sizes of 1.22 and 0.28 μm, respectively (Figs. 1(b) and 1(c), and Figs. S1(b) and S1(c) in the ESM). By inverting the tubes holding MXene inks, we can clearly see the difference in viscosity of the three samples: the L-MXene ink with the largest lateral size showed the highest viscosity while the S-MXene inks with smaller sizes showed higher flowability (Figs. 1(d)–1(f)). The size-dependent viscosity of MXene inks can be attributed to the transition from isotropic phase to nematic phase with increasing size of MXene nanosheets [32]. According to Onsager theory, an isotropic phase with randomly oriented nanoflakes can transform into nematic phase beyond critical transition concentration (C_t) [33]. For MXene solution, the C_t value increases with decreasing lateral dimension of MXene nanosheets [32]. Thus, the S-MXene inks tend to form an isotropic phase, exhibiting a liquid-like behavior with low viscosity, while the L-MXene ink forms a nematic phase, exhibiting gel-like behavior with higher viscosity [34]. To further confirm this size-dependent viscosity variation, rheological properties of L-MXene, S2-MXene and S1-MXene inks were measured. As depicted in Fig. 1(g), all of the three inks showed shear thinning behavior as the shear rate increases, which is a typical behavior of non-Newtonian fluid. Notably, the L-MXene ink showed a significantly higher viscosity of 9677 Pa·s compared with S1-MXene ink (180 Pa·s) at low shear rate of 0.01 s^{-1}, demonstrating the better extrusion performance of L-MXene ink to realize high-resolution printing. As can be seen from the energy storage modulus (G') and loss modulus (G'') curves of the inks in Fig. 1(h), the L-MXene ink exhibited a yield stress of ~ 246 Pa, which was much higher than that of S1-MXene ink (3 Pa) and S2-MXene ink (16 Pa). More specifically, the higher value of G' compared with G'' in the region below the yield point indicates a solid-like behavior dominated by elastic deformation. The high G', G'' values and G'/G'' ratio of L-MXene inks improve the instantaneous curing of the ink after continuous extrusion and shear removal during the screening printing process. When the shear stress is increased beyond that point, the G'' value decreased more abruptly than G', yielding a G'/G'' ratio less than 1, which indicates a liquid-like behavior in the high shear stress area. This region is thus favorable for the continuous extrusion of MXene inks from the screen onto the target substrate. By alternating between low (0.1 s^{-1}) and high (100 s^{-1}) shear rates for the MXene inks, it was found that the apparent viscosity of the inks decreased abruptly as the shear rate increased from 0.1 to 100 s^{-1}, and can be recovered instantaneously when the shear rate dropped back to 0.1 s^{-1} (Fig. 1(i)). This highly elastic rheological property of L-MXene ink is essential to maintain the structure integrity of printed patterns and prevent short circuits.

2.2 Printing performance of MXene ink

Based on the above analyses, the L-MXene ink with the highest viscosity was chosen as the prime sample for screen printing test

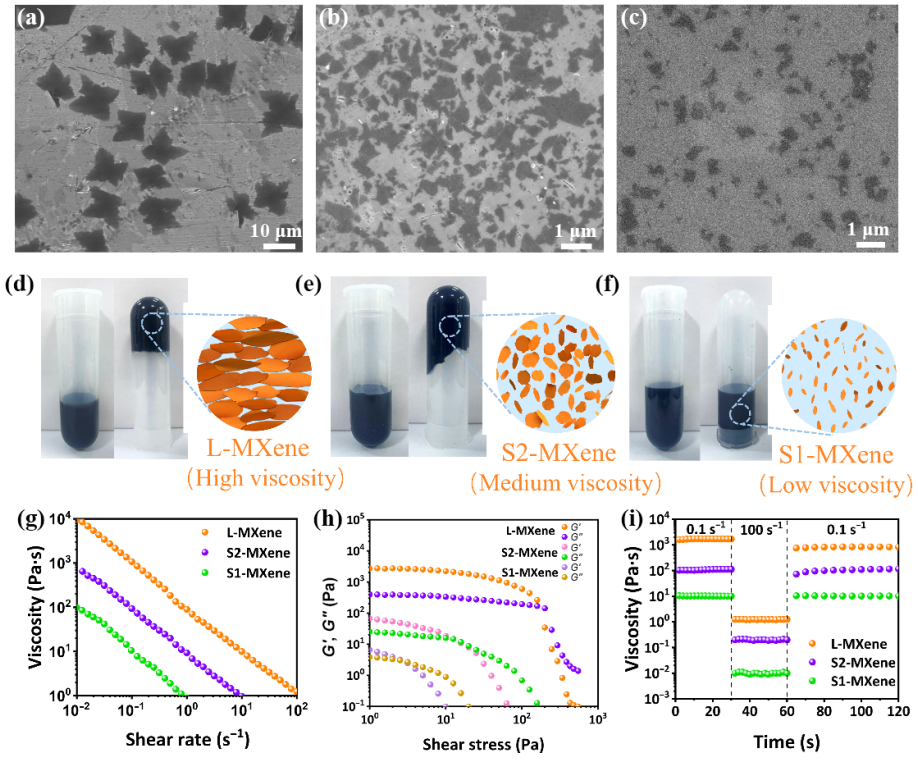

Figure 1 Comparison of L-MXene, S2-MXene and S1-MXene inks. SEM images of L-MXene (a), S2-MXene (b) and S1-MXene (c) inks. (d)–(f) Digital photographs of the obtained MXene inks in upright and inverted states showing different viscosities. Insets: graphical illustrations of the sizes and distributions of corresponding nanosheets. (g) Viscosity as a function of shear rate for L-MXene ink, S2-MXene ink and S1-MXene ink. (h) Storage modulus (G') and loss modulus (G'') as a function of shear stress for L-MXene ink, S2-MXene ink and S1-MXene ink. (i) Viscosity variation of L-MXene ink, S2-MXene ink and S1-MXene ink under changing shear rates.

with the S-MXene inks as controls. Predictably, the printing quality depends heavily on the viscosity of the inks (Fig. 2(a)). The L-MXene can be smoothly extruded from the screen mesh to various substrates, thus realizing sharp edges and intact structures of the printed patterns while the pattern printed with S1-MXene ink was incomplete with fuzzy edges (Figs. 2(b) and 2(c)). The resolution of the pattern printed on polyethylene terephthalate (PET) substrate with L-MXene ink can reach 0.05 mm as depicted in Fig. 2(d). It is also worth noting that the printing can be easily adapted to different flexible substrates including polyimide (PI) and photographic paper (Figs. 2(e) and 2(f)).

We further explored the influence of printing times and number of screen mesh on electrical conductivity to obtain MXene film with the optimized conductivity. Figures 3(a)–3(c) show square resistance, thickness and conductivity of printed L-MXene films as a function of printing times using 80 mesh patches. As printing times increased, the square resistance decreased (Fig. 3(a)) while the thickness increased (Fig. 3(b)). The coeffect of these two factors leads to an optimal conductivity with printing times of 3 (Fig. 3(c)). We then investigated the influence of mesh number on the electrical conductivity by keeping the printing times at 3. With increasing mesh number, the square resistance gradually increased (Fig. 3(d)) while the thickness of the film gradually decreased (Fig. 3(e)). As a result, the highest conductivity was achieved when the mesh number is between 60 and 80 (Fig. 3(f)). Thus, printing times of 3 and mesh number of 80 were selected for subsequent printing. Cross-sectional SEM images of the printed L-MXene film under optimized conditions (printing times = 3, mesh number = 80) showed a thickness of approximately 6 μm (Fig. S2(a) in the ESM) with smooth and continuous surface (Fig. S2(b) in the ESM). The electrical conductivity of the film obtained by four-point probe system was 1.67×10^5 S/m, which is the highest among the reported conductivity values for MXene-based films (Fig. 3(g)) [17, 20, 21, 25–29, 35–39], and is also higher than the control samples printed with S2- and S1-MXene inks (Fig. 3(h)). The high electrical conductivity of the film printed with L-MXene could be attributed to the more complete conductive network with less edge defects in large MXene flakes compared to smaller ones as illustrated in Fig. 3(i) as well as lower oxidation degree of the large flakes [40].

2.3 Fabrication of MXene-based RFID tag antenna

Utilizing the high electrical conductivity and flexible nature of the printed MXene films, we proposed an MXene-based RFID tag which is widely used in daily life (Fig. 4(a)). The RFID tag antenna is designed to work within the frequency range of 800–1000 MHz and the corresponding skin depth is within the range of 48.8–43.6 nm which is far below the thickness of the printed film of 6 μm, thus guarantees the proper flow of current. The simulated current distribution of the designed RFID antenna shown in Figs. 4(b) and 4(c) presents antennas fabricated with L-MXene inks via screen printing. It can be seen that the printed antennas have excellent flexibility and conform well to the substrate, which are essential properties for applications in flexible electronic devices.

The measured reading distance results of the RFID antennas printed on PI, PET, and photographic paper substrates are shown in Fig. 4(d) demonstrating a maximum reading distance of ~ 8 m on PI substrate. This is comparable to the previously reported reading distance of MXene-based RFID antennas [7, 30]. Regarding the differences in reading distance when printed on

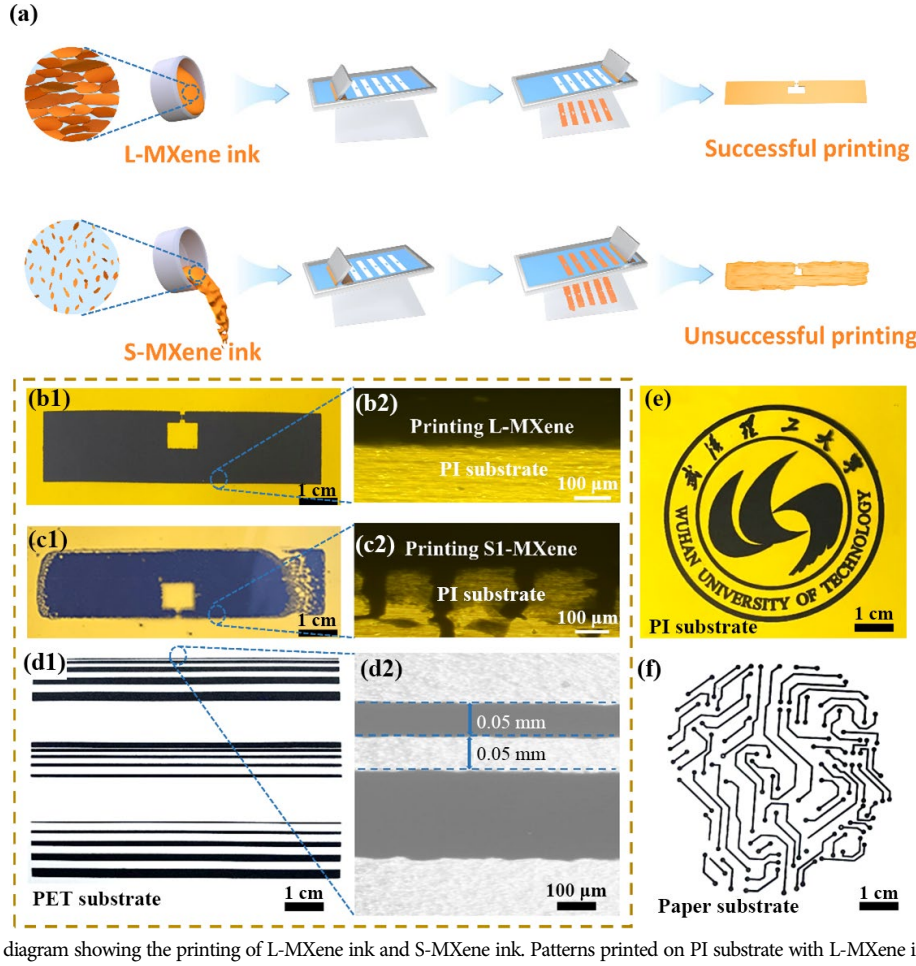

Figure 2 (a) Schematic diagram showing the printing of L-MXene ink and S-MXene ink. Patterns printed on PI substrate with L-MXene ink (b) and S1-MXene ink (c) showing different printing qualities. (d) Lines printed on PET substrate with L-MXene ink with line width and separation down to 0.05 mm. Complex patterns printed on PI (e) and photographic paper (f) substrates using L-MXene ink.

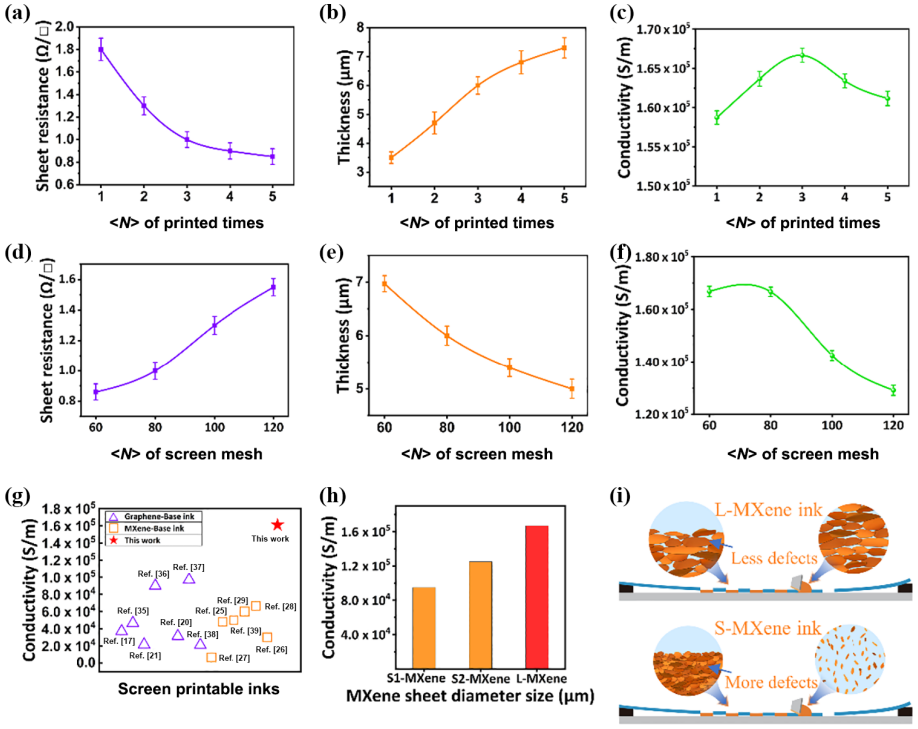

Figure 3 (a)–(c) Square resistance, thickness and conductivity of printed L-MXene films as a function of printing times (mesh number = 80). (d)–(f) Square resistance, thickness and conductivity of printed L-MXene films as a function of mesh number (printing times = 3). (g) Comparison of electrical conductivity of L-MXene film in this work and other reported values. (h) Comparison of electrical conductivity of L-MXene, S2-MXene and S1-MXene screen-printed films. (i) Graphical illustration of possible reasons for the differences in electrical conductivity of L-MXene and S-MXene screen-printed films.

various substrates, there are two possible explanations: (1) the difference in contact resistance between the substrates and the MXene films/chip; (2) different wettability of the substrates leads to variation in local coverage and thus affects the overall conductivity [41].

Reading distances were also measured before and after bending the RFID antenna for 1000 times to investigate the mechanical stability. As shown in Fig. 4(e), the reading distance decreases slightly after bending tests but is still within operational range, indicating the continuity of the internal current even after 1000 cycles of bending and stretching tests (Fig. S3 in the ESM). The decrease in reading distance can be ascribed to the deteriorating contact between the chip and the antenna during repetitive bending. Figure 4(f) shows the comparison of reading distance between the RFID antenna printed on PI substrate under flat and bending conditions (Fig. S4 in the ESM). When bending at 45°, the reading distance decreased slightly within the entire frequency range due to the decreased effective radiation area of the antenna. However, benefiting from the superb flexibility and conformality of the MXene film, the rear reading distance can still reach 7 m with no shift of the frequency for maximum reading distance [42]. These results validate the excellent mechanical flexibility of the MXene-based tags, which is highly demanded for applications in wearable electronics and conformal antennas.

3 Conclusions

In summary, we demonstrated additive-free MXene inks with high conductivity and viscosity suitable for screen printing of MXene-based wireless electronics. We find that by regulating the size of MXene nanosheets, MXene inks with different rheological properties can be obtained. Namely, the larger MXene nanosheets endow MXene inks with higher viscosity and higher conductivity in the absence of additives. The MXene film printed under the optimal conditions showed ultrafine resolution of 0.05 mm and high conductivity of 1.67×10^5 S/m. Further, RFID tag antennas were batch-fabricated based on the additive-free MXene inks via screen printing and demonstrated reading distance over 8 m with superb flexibility and mechanical stability. This work unveils a size-dependent behavior of viscosity and conductivity for MXene inks, thus providing a new strategy for the scalable and low-cost manufacture of MXene-based wireless electronics via screen printing technology.

4 Methods

4.1 Chemicals

2D titanium carbide MXenes with different nanosheet sizes were purchased from Sanya Hanene Graphene Technology Research Institute Co., Ltd. All chemicals were used as received and deionized water was used in the experiments.

4.2 Preparation of MXene ink

Three MXene solutions with different sizes of nanosheets were centrifuged at 9000 rpm for 30 min to get concentrated solutions. By discarding the supernatant and diluting the solid residues to 100 mg/mL in deionized water, three types of MXene inks (denoted as L-, S2- and S1-MXene ink for nanosheet sizes from largest to smallest, respectively) were obtained and ready for further characterization.

4.3 Fabrication of RFID tag antenna

The RFID patterns were screen printed on different flexible substrates (PI, PET and photographic paper) using MXene ink through an air-breathing flat screen printing machine (SY-500P, Sanyang Printing Equipment Products Co., Ltd). After dried at room temperature, the RFID tags were packaged using an electronic tag packaging machine (TG320, Tagrid Technology Co., Ltd.).

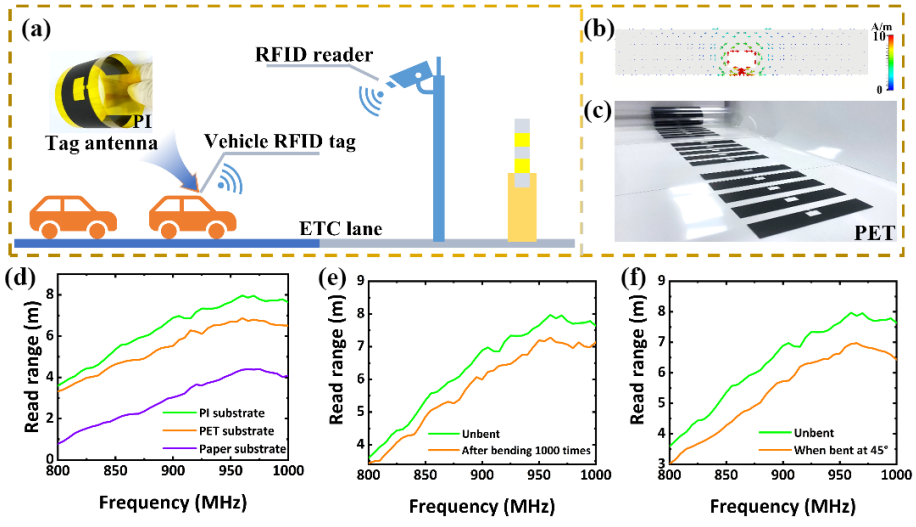

Figure 4 MXene-based RFID antenna via screen printing. (a) Display of the application of RFID antenna in electronic toll collection (ETC). The upper left illustration shows the antenna printed on PI substrate. (b) Simulated current distribution of the proposed RFID antenna. (c) Batch screen-printed antennas on PET substrate. (d) Reading distance results of antennas printed on different substrates. (e) Reading distances of the RFID antenna printed on PI substrate before and after 1000 times of bending. (f) Reading distances of the RFID antenna printed on PI substrate under flat and bending states.

4.4 Characterization

SEM images were taken with Zeiss Ultra Plus SEM. The viscosity and elastic modulus of MXene inks were evaluated by Dynamic Shear rheometer (Anton Paar, SmartPave 92). The reading range of RFID antenna was tested by RFID comprehensive tester (Ruihui Electronics, Shanghai Co., Ltd.). To determine the conductivity of the obtained MXene films, a four-point probe instrument RTS-9 with probing distance of 1 mm was applied to determine the resistance and the thickness was measured using a spiral micrometer. The conductivity was then calculated by the following equation:

$$\sigma = \frac{1}{hR_s} \quad (1)$$

where σ is the conductivity, h is the thickness of printed film, R_s is the sheet resistance.

The skin depth of the MXene film can be obtained by the following equation:

$$\delta = \sqrt{\frac{2}{\omega\mu\sigma}} \quad (2)$$

in which δ is the skin depth, ω is the angular frequency, μ is the permeability and σ is the conductivity.

Acknowledgements

This work was supported by the National Natural Science Foundation of China (No. 22279097), the Hainan Provincial Joint Project of Sanya Yazhou Bay Science and Technology City (No. 520LH054), and the Fundamental Research Funds for the Central Universities (WUT: 2021IVA66).

Electronic Supplementary Material: Supplementary material (size distribution histograms; cross-sectional and top-view SEM images of L-MXene film; experimental setup of the bending test of the antenna; digital photograph showing the antenna conforms to a plastic bottle and setup of read range test) is available in the online version of this article at https://doi.org/10.1007/s12274-023-5762-3.

References

[1] Liang, C.; Qiu, K. F.; Zhang, Z.; Yang, J.; Li, Y. Z.; Hu, J. J. Towards robust and stealthy communication for wireless intelligent terminals. *Int. J. Intell. Syst.* **2022**, *37*, 11791–11814.

[2] Oteafy, S. M. A.; Hassanein, H. S. IoT in the fog: A roadmap for data-centric IoT development. *IEEE Commun. Mag.* **2018**, *56*, 157–163.

[3] Xu, L. Q.; Tang, Y. Z.; Zhang, C.; Liu, F. H.; Chen, J. K.; Xuan, W. P.; Jin, H.; Ye, Z.; Cao, Z.; Li, Y. B. et al. Fully self-powered instantaneous wireless liquid level sensor system based on triboelectric nanogenerator. *Nano Res.* **2022**, *15*, 5425–5434.

[4] Wang, W. T.; Lu, L. S.; Lu, X. Y.; Liang, Z. B.; Lin, H. H.; Li, Z. H.; Wu, X. H.; Lin, L. H.; Xie, Y. X. Scorpion-inspired dual-bionic, microcrack-assisted wrinkle based laser induced graphene-silver strain sensor with high sensitivity and broad working range for wireless health monitoring system. *Nano Res.* **2023**, *16*, 1228–1241.

[5] Khan, Y.; Thielens, A.; Muin, S.; Ting, J.; Baumbauer, C.; Arias, A. C. A new frontier of printed electronics: Flexible hybrid electronics. *Adv. Mater.* **2020**, *32*, 1905279.

[6] Li, D. D.; Lai, W. Y.; Zhang, Y. Z.; Huang, W. Printable transparent conductive films for flexible electronics. *Adv. Mater.* **2018**, *30*, 1704738.

[7] Shao, Y. Z.; Wei, L. S.; Wu, X. Y.; Jiang, C. M.; Yao, Y.; Peng, B.; Chen, H.; Huangfu, J. T.; Ying, Y. B.; Zhang, C. J. et al. Room-temperature high-precision printing of flexible wireless electronics based on MXene inks. *Nat. Commun.* **2022**, *13*, 3223.

[8] Zhu, H. W.; Gao, H. L.; Zhao, H. Y.; Ge, J.; Hu, B. C.; Huang, J.; Yu, S. H. Printable elastic silver nanowire-based conductor for washable electronic textiles. *Nano Res.* **2020**, *10*, 2879–2884.

[9] Zhang, Y. F.; Wang, C.; Dong, X. Y.; Jiang, H. M.; Hu, T.; Meng, C. G.; Huang, C. Alkali etching metal silicates derived from bamboo leaves with enhanced electrochemical properties for solid-state hybrid supercapacitors. *Chem. Eng. J.* **2021**, *417*, 127964.

[10] Lin, Y.; Li, Q. S.; Ding, C., Wang, J. Y.; Yuan, W.; Liu, Z. Y.; Su, W. M.; Cui, Z. High-resolution and large-size stretchable electrodes based on patterned silver nanowires composites. *Nano Res.* **2022**, *15*, 4590–4598.

[11] Wang, G. D.; Adil, M. A.; Zhang, J. Q.; Wei, Z. X. Large-area organic solar cells: Material requirements, modular designs, and printing methods. *Adv. Mater.* **2019**, *31*, 1805089.

[12] Ma, R. H.; Wang, C. F.; Yan, W.; Sun, M. Z.; Zhao, J. X.; Zheng, Y. T.; Li, X.; Huang, L. B.; Chen, B.; Wang, F. et al. Interface synergistic effects induced multi-mode luminescence. *Nano Res.* **2022**, *15*, 4457–4465.

[13] Kokkonen, M.; Talebi, P.; Zhou, J.; Asgari, S.; Soomro, S. A.; Elsehrawy, F.; Halme, J.; Ahmad, S.; Hagfeldt, A.; Hashmi, S. G. Advanced research trends in dye-sensitized solar cells. *J. Mater. Chem. A* **2021**, *9*, 10527–10545.

[14] Liang, J. J.; Tong, K.; Pei, Q. B. A water-based silver-nanowire

screen-print ink for the fabrication of stretchable conductors and wearable thin-film transistors. *Adv. Mater.* **2016**, *28*, 5986–5996.
[15] Jun, H. Y.; Lee, E. J.; Ryu, S. O. Synthesis and characterization of copper ink and direct printing of copper patterns by inkjet printing for electronic devices. *Curr. Appl. Phys.* **2020**, *20*, 853–861.
[16] Gemeiner, P.; Pavličková, M.; Hatala, M.; Hvojnik, M.; Homola, T.; Mikula, M. The effect of secondary dopants on screen-printed PEDOT: PSS counter-electrodes for dye-sensitized solar cells. *J. Appl. Polym. Sci.* **2022**, *139*, 51929.
[17] Pan, K. W.; Fan, Y. Y.; Leng, T.; Li, J. S.; Xin, Z. Y.; Zhang, J. W.; Hao, L.; Gallop, J.; Novoselov, K. S.; Hu, Z. R. Sustainable production of highly conductive multilayer graphene ink for wireless connectivity and IoT applications. *Nat. Commun.* **2018**, *9*, 5197.
[18] Chen, K.; Gao, W.; Emaminejad, S.; Kiriya, D.; Ota, H.; Nyein, H. Y. Y.; Takei, K.; Javey, A. Printed carbon nanotube electronics and sensor systems. *Adv. Mater.* **2016**, *28*, 4397–4414.
[19] Goh, Y.; Lauro, S.; Barber, S. T.; Williams, S. A.; Trabold, T. A. Cleaner production of flexographic ink by substituting carbon black with biochar. *J. Clean. Prod.* **2021**, *324*, 129262.
[20] Ding, H.; He, P.; Yang, J. X.; Liu, C. G.; Zhao, H.; Derby, B. Water-based highly conductive graphene inks for fully printed humidity sensors. *J. Phys. D Appl. Phys.* **2020**, *53*, 455304.
[21] Liu, L. X.; Shen, Z. G.; Zhang, X. J.; Ma, H. Highly conductive graphene/carbon black screen printing inks for flexible electronics. *J. Colloid Interface Sci.* **2021**, *582*, 12–21.
[22] Mohammadi, A. V.; Rosen, J.; Gogotsi, Y. The world of two-dimensional carbides and nitrides (MXenes). *Science* **2021**, *372*, eabf1581.
[23] Jiang, J. Z.; Bai, S. S.; Zou, J.; Liu, S.; Hsu, J. P.; Li, N.; Zhu, G. Y.; Zhuang, Z. C.; Kang, Q.; Zhang, Y. Z. Improving stability of MXenes. *Nano Res.* **2022**, *15*, 6551–6567.
[24] Yu, L. H.; Fan, Z. D.; Shao, Y. L.; Tian, Z. N.; Sun, J. Y.; Liu, Z. F. Versatile N-doped MXene ink for printed electrochemical energy storage application. *Adv. Energy Mater.* **2019**, *9*, 1901839.
[25] Wu, H.; Xie, Y. M.; Ma, Y. A.; Zhang, B. B.; Xia, B.; Zhang, P. X.; Qian, W.; He, D. P.; Zhang, X.; Li, B. W. et al. Aqueous MXene/xanthan gum hybrid inks for screen-printing electromagnetic shielding, joule heater, and piezoresistive sensor. *Small* **2022**, *18*, 2107087.
[26] Li, X.; Sun, R. J.; Pan, J. Y.; Shi, Z. H.; Lv, J. J.; An, Z. J.; He, Y.; Chen, Q. M.; Han, R. P. S.; Zhang, F. N. et al. All-MXene-printed RF resonators as wireless plant wearable sensors for *in situ* ethylene detection. *Small*, in press, DOI: 10.1002/smll.202207889.
[27] Chen, Y. A.; Li, Y. H.; Liu, Y.; Chen, P.; Zhang, C. Z.; Qi, H. S. Holocellulose nanofibril-assisted intercalation and stabilization of $Ti_3C_2T_x$ MXene inks for multifunctional sensing and EMI shielding applications. *ACS Appl. Mater. Interfaces* **2021**, *13*, 36221–36231.
[28] Deng, Z. M.; Li, L. L.; Tang, P. P.; Jiao, C. Y.; Yu, Z. Z.; Koo, C. M.; Zhang, H. B. Controllable surface-grafted MXene inks for electromagnetic wave modulation and infrared anti-counterfeiting applications. *ACS Nano* **2022**, *16*, 16976–16986.
[29] Abdolhosseinzadeh, S.; Schneider, R.; Verma, A.; Heier, J.; Nüesch, F.; Zhang, C. F. Turning trash into treasure: Additive free MXene sediment inks for screen-printed micro-supercapacitors. *Adv. Mater.* **2020**, *32*, 2000716.
[30] Sarycheva, A.; Polemi, A.; Liu, Y. Q.; Dandekar, K.; Anasori, B.; Gogotsi, Y. 2D titanium carbide (MXene) for wireless communication. *Sci. Adv.* **2018**, *4*, eaau0920.
[31] Huang, L.; Huang, Y.; Liang, J. J.; Wan, X. J.; Chen, Y. S. Graphene-based conducting inks for direct inkjet printing of flexible conductive patterns and their applications in electric circuits and chemical sensors. *Nano Res.* **2011**, *4*, 675–684.
[32] Zhang, J. Z.; Uzun, S.; Seyedin, S.; Lynch, P. A.; Akuzum, B.; Wang, Z. Y.; Qin, S.; Alhabeb, M.; Shuck, C. E.; Lei, W. W. et al. Additive-free MXene liquid crystals and fibers. *ACS Cent. Sci.* **2020**, *6*, 254–265.
[33] Onsager, L. The effects of shape on the interaction of colloidal particles. *Ann. New York Acad. Sci.* **1949**, *51*, 627–659.
[34] Tezel, G. B.; Arole, K.; Holta, D. E.; Radovic, M.; Green, M. J. Interparticle interactions and rheological signatures of $Ti_3C_2T_z$ MXene dispersions. *J. Colloid Interface Sci.* **2022**, *605*, 120–128.
[35] Leng, T.; Pan, K. W.; Zhang, Y. W.; Li, J. S.; Afroj, S. L.; Novoselov, K. S.; Hu, Z. R. Screen-printed graphite nanoplate conductive ink for machine learning enabled wireless radiofrequency-identification sensors. *ACS Appl. Nano Mater.* **2019**, *2*, 6197–6208.
[36] Lin, M. Y.; Gai, Y. Z.; Xiao, D.; Tan, H. J.; Zhao, Y. P. Preparation of pristine graphene paste for screen printing patterns with high conductivity. *Chem. Phys. Lett.* **2018**, *713*, 98–104.
[37] Xu, L. Y.; Wang, H. P.; Wu, Y. D.; Wang, Z. A.; Wu, L. X.; Zheng, L. H. A one-step approach to green and scalable production of graphene inks for printed flexible film heaters. *Mater. Chem. Front.* **2021**, *5*, 1895–1905.
[38] Wang, J. J.; Du, Y.; Qin, J.; Wang, L.; Meng, Q. F.; Li, Z. Y.; Shen, S. Z. Flexible thermoelectric reduced graphene oxide/Ag_2S/methyl cellulose composite film prepared by screen printing process. *Polymers* **2022**, *14*, 5437.
[39] Zheng, S. H.; Wang, H.; Das, P.; Zhang, Y.; Cao, Y. X.; Ma, J. X.; Liu, S. Z.; Wu, Z. S. Multitasking MXene inks enable high-performance printable microelectrochemical energy storage devices for all-flexible self-powered integrated systems. *Adv. Mater.* **2021**, *33*, 2005449.
[40] Wan, S. J.; Li, X.; Chen, Y.; Liu, N. N.; Wang, S. J.; Du, Y.; Xu, Z. P.; Deng, X. L.; Dou, S. X.; Jiang, L. et al. Ultrastrong MXene films via the synergy of intercalating small flakes and interfacial bridging. *Nat. Commun.* **2022**, *13*, 7340.
[41] Arapov, K.; Jaakkola, K.; Ermolov, V.; Bex, G.; Rubingh, E.; Haque, S.; Sandberg, H.; Abbel, R.; De With, G.; Friedrich, H. Graphene screen-printed radio-frequency identification devices on flexible substrates. *Phys. Status Solidi. Rapid Res. Lett.* **2016**, *10*, 812–818.
[42] Zhang, B. H.; Wang, Z.; Song, R. G.; Fu, H. Q.; Zhao, X.; Zhang, C.; He, D. P.; Wu, Z. P. Passive UHF RFID tags made with graphene assembly film-based antennas. *Carbon* **2021**, *178*, 803–809.